PAPER

Check for updates

Synthesis and efficacy of norfloxacin loaded onto magnetic hydrogel nanocomposites

Nehal Salahuddin, [ID] * Ahmed Rehab [ID] * and Sahar Emad

A targeted drug delivery system based on biocompatible magnetic hydrogel nanocomposites consisting of poly[oligo(oxyethylene methacrylate)] anchored Fe_3O_4 nanoparticles was synthesized. The characteristics, thermal properties, morphology and magnetic properties were studied by XRD, FT-IR, TGA, SEM, TEM and VSM. A norfloxacin (NOR) anti-bacterial agent with a potential antitumor activity was immobilized into hydrogels, Fe_3O_4 nanoparticles and their magnetic hydrogel nanocomposites. The *in vitro* drug release manner of NOR was explored at different temperatures and pH values. The behavior of the drug release has been studied *via* different kinetic models. The antibacterial efficacy was tested against *Streptococcus*, *Staphylococcus aureus*, *Kelebsella pneumonia* and *Escherichia coli via* well diffusion method, and showed significant activity compared to the unloaded drug. Furthermore, an antitumor efficacy against HCT-116, HepG-2, PC3 and MCF-7 cancer cells revealed the highest cytotoxic efficacy with no influence on healthy cells. These nanodrugs, retaining both antibacterial and anticancer efficacy, have a talented therapeutic potential because of their selective cytotoxicity, connected with the ability to minimize the risk of bacterial infection in a cancer patient who is frequently immunocompromised.

1 Introduction

Hydrogels have advantages for different biomedical applications because of their inherent biocompatibility and their similarity to natural soft tissues, due to their flexible, soft nature, and ability to import a high percentage of water.[1] Hydrogels have a high porosity structure, which allow the drugs to be loaded into the gel matrix. Afterwards, the drugs are released at a rate depending on the diffusion coefficient of the small molecule across the gel network.[2] The biocompatibility of hydrogels is reflected by their successful use in peritoneum[3] *in vivo*, and its ability to be biodegradable by environmental factors (temperature, pH), hydrolysis or enzymatic analysis.[2] The relative deformability of hydrogels also makes it adaptable to the shape of the surface to which it will be applied.[2] In the later context, some hydrogels of bio-adhesive properties may be beneficial in applying them to non-horizontal surfaces, or by transferring them at the application site.[2]

Recently, hydrogel nanocomposites have been applied in various biomedical applications, such as cancer treatment and drug delivery.[4] Lately, the magnetic hydrogel has witnessed great advancement, which can comply to an external magnetic field.[5] Regarding old-style stimuli, such as temperature and pH, the magnetic response is more appropriate for monitoring delivery because of its exceptional characteristics, which include remote operation, easy management control and rapid

Chemistry Department, Faculty of Science, Tanta University, Tanta 31527, Egypt. E-mail: ahmed.fathalla@science.tanta.edu.eg; nehal.attaf@science.tanta.edu.eg

response.[6] In the hyperthermia technique, biocompatible magnetic gel composites that are made by incorporating magnetic nanoparticles (MNPs) into polymer hydrogel matrices were used.[7,8]

Magnetite nanoparticles (MNPs) is a kind of smart nanomaterials with super paramagnetism, magnetic response, large specific surface area and small particle size.[9] Fe_3O_4-NPs should be biodegradable and biocompatible to reduce their toxicity.[10–12] Because of the MNPs' properties, they can easily reach the position of the injury.[13] MNPs were used as drugs delivery agents, so that drugs may be directed towards the targeted place *in vivo* through applying an external magnetic field.[14] This participates in overcoming the difficulties accompanying the traditional chemotherapeutic agents, including rapid clearance, poor solubility under aqueous conditions and lack of selectivity, which subsequently lead to nonspecific toxicity towards normal cells.[15] Drug-loaded Fe_3O_4-NPs can pile up at the tumor site through the assistance of an external magnetic field.[12] This leads to increasing the efficacy of releasing drugs without any harm to healthy cells.[12]

However, because of some toxicity associated with the use of MNPs, several limitations have been applied in their application.[16] Therefore, the surface coating of MNPs and size control can improve the magnetic behavior and minimize toxicity.[16] The utilization of MNPs in drug release field is the most promising application, particularly for cancer treatment.[17] This innovative strategy consists of loading magnetic systems with the drug, which may be directed to the target using an external magnetic field.[18,19] MNPs release the drugs once they reach the target

under the action of alternating magnetic field.[17] MNPs have shortcomings related to the loading of a small amount of drugs associated with each NP. This shortcoming implies the necessity of injecting large concentrations of NPs for achieving the targeted treatment.[17]

Some of the incurred issues may be dealt with through introducing MNPs into a hydrogel.[17] There are many methods suggested for using metal oxide nanoparticles in hydrogels.[20,21] Most magnetic hydrogels are invented by *in situ* precipitation method[22] or by blending method.[8] Cross-linked structural magnetic hydrogels were prepared hierarchically by encapsulating MNPs into micelles, followed by embedding in a polymer matrix.[23] Functionalized MNPs were used as crosslinked chemical elements to form hydrogel networks[24,25] through modifying the surface of the nanoparticles that ensure the covalent conjugation of a hydrogel matrix.[5] Interestingly, the introduction of covalent bonds between the hydrogel network and MNPs improved the MNP dispersion inside the hydrogel matrix.[5] Incorporating iron oxide nanoparticles into hydrogels may lead to producing tunable nanocomposites, which may be controlled remotely through an external magnetic field.[26–30]

Magnetic hydrogel nanocomposites, in addition to being used with drug delivery, can be used in hyperthermia cancer treatment in order to heat cancer cells and tissues, making them more sensitive to chemotherapy or radiation.[7,31,32] In magnetic targeting vehicles, there is no need for any additional chemical additives to induce the response; only an external magnetic field is needed compared to other target compounds.[5]

It is challenging to design drug carriers that have all of the desired characteristics. Overcoming all barriers and improving the accumulation are always a critical mission for drug carriers, and it is very important to induce the release after accumulation by increasing the functionality of the drug carriers.[33] In particular, spatially variant magnetic fields have been used to encourage the accumulation of drug-loaded MNPs at target sites, while time-variant magnetic fields have been used to induce drug release from thermally sensitive nanocarriers. This work was aimed to design targeted drug delivery systems based on hydrogels and magnetic hydrogel nanocomposites to improve the functionality of the carriers. These systems consist of poly[oligo(oxyethylene methacrylate)]-anchored MNPs *via in situ* polymerization in the presence of MNPs, followed by the loading of norfloxacin (NOR) as an antibacterial agent with potential antitumor activity. In addition, the release of the drug under different conditions, antibacterial activity and potential antitumor activity will be examined under different conditions.

2 Materials and methods

Ferric chloride [$FeCl_3$] (Alpha Chemica), ferrous sulfate [$FeSO_4 \cdot 7H_2O$] (Oxford Lab Chem, India), sodium hydroxide [NaOH] (Bio Chem), HCl (Elnasr Pharmaceuticals Chemicals Co.), ethanol (Bio Chem), ammonium peroxydisulfate and potassium persulfate were used as received from Riedel-de Haen AG, Seelze-Hannover. Commercial di(oxyethylene) methacrylate (DOEMA) and tetra(oxyethylene) methacrylate (TOEMA) were obtained from Nippon Oil and Fats Co., Japan without
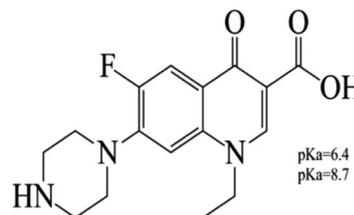

Fig. 1   Structure of norfloxacin.

further treatment. *N,N'*-Methylenebisacrylamide (MBAA, Aldrich) and norfloxacin, NOR, (Epico, Egypt) were used as received. The empirical formula of NOR is $C_{16}H_{18}FN_3O_3$ and the structural formula is shown in Fig. 1.

2.1. Synthesis of MNPs

The synthesis of MNPs was carried out by dissolving a mixture of 8.125 g $FeCl_3$ and 6.950 g of $FeSO_4 \cdot 7H_2O$ (2 : 1 molar ratio) in 50 mL deoxygenated distilled water under N_2 atmosphere. After stirring for 1 h, the precipitate was achieved by adding 2 M NaOH solution dropwise under vigorous stirring at 30 °C. The mixture was heated and kept at 70 °C (pH $\approx$ 12) under vigorous stirring for 5 h. Then, the system was cooled to $\approx$ 25 °C and the black precipitate was separated, followed by washing with deoxygenated distilled water and ethanol. Finally, MNPs was dried at 60–70 °C.[34]

2.2. Synthesis of polymeric hydrogels ($I_{a,b}$)

The hydrogels were synthesized through radical polymerization by dissolving oligo(oxyethylene methacrylates) (PE-90 or PE-200) monomers in 50 mL distilled water in the presence of 1% potassium persulfate as an initiator with stirring, followed by heating at 80–90 °C for 6–8 hours. The obtained hydrogels were removed by decantation, washed with ethanol three times, and finally dried under reduced pressure at 30–40 °C for 24 h to obtain the hydrogels ($I_{a,b}$), as shown in Scheme 1.
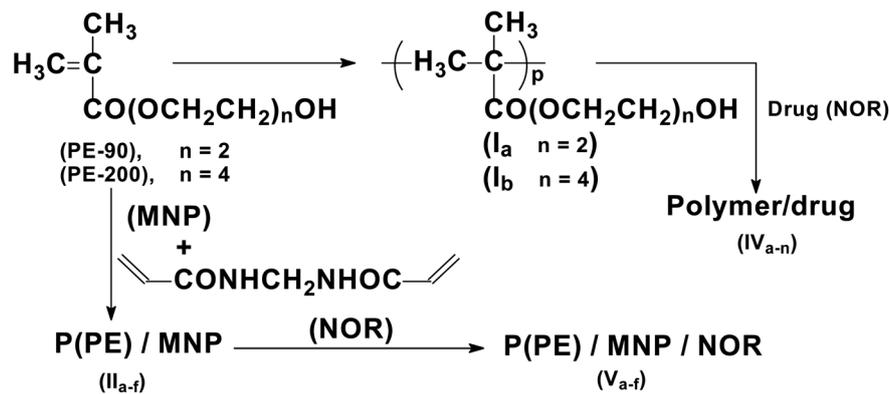
2.3. Synthesis of magnetic hydrogel nanocomposites (II_{a-f})

Magnetic hydrogel nanocomposites were synthesized by *in situ* polymerization, as shown in Scheme 1. Accordingly, a mixture of 5 g monomers (PE-90), 0.195 g of *N,N*-methylenbisacrylamide (crosslinker) and 0.25 g (5 w/w%) of MNPs were dispersed under nitrogen in 40 mL distilled water using a sonication bath for 30 minutes. Then, 0.074 g of potassium persulfate solution in 10 mL of distilled water was added to the previous mixture with stirring. After that, the mixture was heated at 80–90 °C for 8 h under nitrogen gas. The obtained nanocomposite was washed with ethanol twice and dried at 30–40 °C under low pressure to produce (II_a). The same procedure was followed using different amounts of MNPs and monomer (PE-200) to produce (II_{b-f}), as in Table 1.

2.4. Loading of NOR on the prepared carriers

A stock solution of the NOR drug was prepared by dissolving 0.04 g in 20 mL of DMSO, and supplemented to 1000 mL with distilled water. After that, successive dilutions were made to

Scheme 1 Synthesis of polymeric hydrogels and magnetic hydrogel nanocomposites.

Table 1 Synthesis of polymeric hydrogels and magnetic hydrogel nanocomposites

Run	Monomer[a]	MNPs	
		Wt (g)	(%)
I_a	DOEMA (PE-90)	—	—
II_a	DOEMA (PE-90)	0.25	5
II_b	DOEMA (PE-90)	0.50	10
II_c	DOEMA (PE-90)	0.75	15
I_b	TOEMA (PE-200)	—	—
II_d	TOEMA (PE-200)	0.25	5
II_e	TOEMA (PE-200)	0.50	10
II_f	TOEMA (PE-200)	0.75	15

[a] Weight of monomer = 5 g.

reach the required concentrations. Then, the drug (NOR) was loaded onto MNPs, hydrogels and their nanocomposites by adding 0.1 g of the sample into 20 mL of NOR solution (16 ppm), followed by stirring, and the precipitate was then collected by centrifuge. The loaded drug was followed by calculating the concentration of supernatant after centrifugation using a UV-visible instrument. The loading (%) was calculated by measuring the absorption at $\lambda_{max} = 274$ nm from the calibration curve of NOR using the following equation:[1]

$$\text{Loading } \% = \frac{\text{mass of drug immoblized on carrier}}{\text{mass of dry carrier}} \quad (1)$$

The data of loading for the hydrogels and their nanocomposites are shown in Table 3. The effect of different conditions, such as the sample structure, temperature, drug concentration and pH of the medium on loading the drug onto hydrogels, was studied and the best conditions were used for loading the drug onto the MNPs and magnetic hydrogel nanocomposites with different MNPs contents. All measurements were made and the mean value is reported.

2.5. Preparation of buffer solutions

The buffer solutions were prepared at different pH values (5.4, 6.7 and 7.4) by mixing 500 mL of 0.1 M Na_2HPO_4 with 500 mL of 0.1 M NaH_2PO_4 solutions. Then, the solution was adjusted to the desired pH values by the addition of 1 M HCl or 1 M NaOH. The buffer solution at pH = 5.4 was chosen to imitate the intracellular pH of tumor tissue (endosomes of cancer tissue). The slightly acidic pH = 6.7 was chosen to simulate the extracellular pH of the tumor tissue, and the slightly basic pH = 7.4 was taken to imitate the body fluid environments and extracellular pH of normal tissue.

2.6. Release study of NOR

The release investigation of norfloxacin was done as follows: concisely, 0.1 g of NOR-loaded carriers were dialyzed by cellulose dialysis tubing. Both of the ends of the dialysis tubing were sealed and suspended in 20 mL buffer. Then, a buffer solution at 37 °C was stirred and a solution was withdrawn at particular intervals of time. The release of NOR was investigated by measuring the UV absorption. The released concentration of NOR was calculated through a calibration curve. The extracted release data were analyzed *in vitro* through fitting them to different kinetics equations in order to study the release mechanism of NOR from its carriers.

2.7. Antibacterial activity

The antibacterial efficacy of the conventional drug, free carriers and NOR-loaded carriers against Gram-negative bacteria (*Kelebsella pneumonia*, *Escherichia coli*) and Gram-positive bacteria (*Staphylococcus aureus*, *Streptococcus*) were tested *via* well diffusion method[35] by pouring a specified amount of the medium at a temperature of 40–50 °C into a Petri plates until it reached a depth of 3–4 mm and left to harden, the suspended microorganisms were prepared to hold 5×10^{-5} CFU mL^{-1}. The tested microorganisms were put into the culture plates, and subsequently allowed to solidify. They were struck with a sterile cork borer (with a diameter of 5.0 mm) to cut regular wells. The open wells were then filled with 0.01 g of the tested compounds, and incubated at 37 °C for 24 hours. The zones of inhibition were evaluated, and the median value was estimated.

2.8. Cytotoxicity assay

Cytotoxic effects of the drug-loaded nanocarriers on various tumors and normal cell lines were detected using the MTT

assay.[36] Selected cell lines, including colorectal carcinoma, HCT 116; ductal carcinoma, MCF-7; hepatocellular carcinoma HepG 2; adenocarcinoma, PC-3 and WISH cell lines were tested, and doxorubicin was used for comparison as a standard cytotoxic agent. Cell lines were cultivated in a 96-well plate in RPMI-1640 medium with 10% fetal bovine serum with 1.0×10^4 cells per well, and then incubated at 37 °C in the presence of 5% CO_2 for 48 h. Cells were treated after incubation with different concentrations of tested samples, and then incubated for 24 h. After that, 20 μl of MTT solution was added at 5 mg mL^{-1}, followed by incubation for 4 h, and dimethyl sulfoxide (DMSO) (100 μl) was then added to each well. Then, the cell viability was measured as (A_{570} of treated samples/A_{570} of untreated sample) × 100.

2.9. Characterization techniques

The FT-IR spectra of the MNPs, hydrogel I_a, I_b and their nanocomposites $II_{(a-f)}$ were done using (Shimadzu FTIR-8101 A), a potassium bromide disc with resolution of 4 cm^{-1} and 64 scans per sample. X-ray diffraction was measured for samples using Philips PW1710 supplied with Cu-Kα radiation ($\lambda = 1.54060$ Å) and current (30 mA), which was recorded at room temperature at a scanning rate of 0.05° min^{-1} to determine their crystallinity. Thermogravimetric analysis (TGA) was conducted on a (TGA-50 Shimadzu) during heating process (25–800 °C) to record the residual weight at a heating rate of 10 °C min^{-1} under N_2 gas. The morphology of MNPs, hydrogel I_a, I_b and their nanocomposites $II_{(a-f)}$ were examined with a scanning electron microscope (SEM) (SU8000 2.0 kV, 4.0 mm, 25.0 K SE(U)) and transmission electron microscope (TEM) (JEM-2100 JEOL). In TEM, the samples were examined using a copper grid (200 mesh) immersed in the dispersion of MNPs and nanocomposites in an ethanolic or distilled water, respectively, after ultrasonication for 30 min. The magnetic properties of the

MNPs and magnetic hydrogel nanocomposites were quantified at room temperature by means of a vibration magnetometer (VSM). The NOR concentration was recorded using UV-Visible spectrophotometry on a Shimadzu 2101PC (UV-1800 double beam) Scanning Spectrophotometer at 200–500 nm.

3 Results and discussion

The objective of the current work is directed to formulate and study the efficacy of MNPs, hydrogel and magnetic hydrogel nanocomposites loaded drug moieties. MNPs were prepared followed by *in situ* radical polymerization of different oxyethylene methacrylates monomers in presence of MNPs using different contents followed by loading NOR onto initially prepared MNPs, polymeric hydrogels and magnetic polymeric hydrogels, as presented in Scheme 1.

The FT-IR spectrum of the Fe_3O_4 nanoparticles (Fig. 2A) shows a strong peak at 578 cm^{-1} due to Fe–O stretching, and bands at 3423 and 1636 cm^{-1} due to the OH stretching and bending, respectively. The XRD pattern (Fig. 2B) of Fe_3O_4 reveals sharp peaks at $2\theta = 29.97°$, 35.37°, 43°, 53.31°, 56.88° and 62.46° that correlates perfectly with the (220), (311), (400), (422), (511) and (440) crystal planes, respectively, according to the Joint Committee on Powder Diffraction Standards (JCPDS no 01-072-2303). The average crystallite size was found to be 23.9 nm as calculated according to the Scherer equation.[37] The morphology of the Fe_3O_4 nanoparticles illustrated in the TEM image (Fig. 2C) displays spherical and cuboid shaped dimensions ranging from 5 to 45 nm, with an average of 15 nm. Fig. 2D shows the isothermal magnetization (M − H) curve at room temperature for MNPs. The M − H curve shows a symmetrical loop of hysteresis in the low field and magnetic field with a saturation magnetization (σ_s) of 60 emu g^{-1}. This behavior indicated that Fe_3O_4 has superparamagnetic behavior.
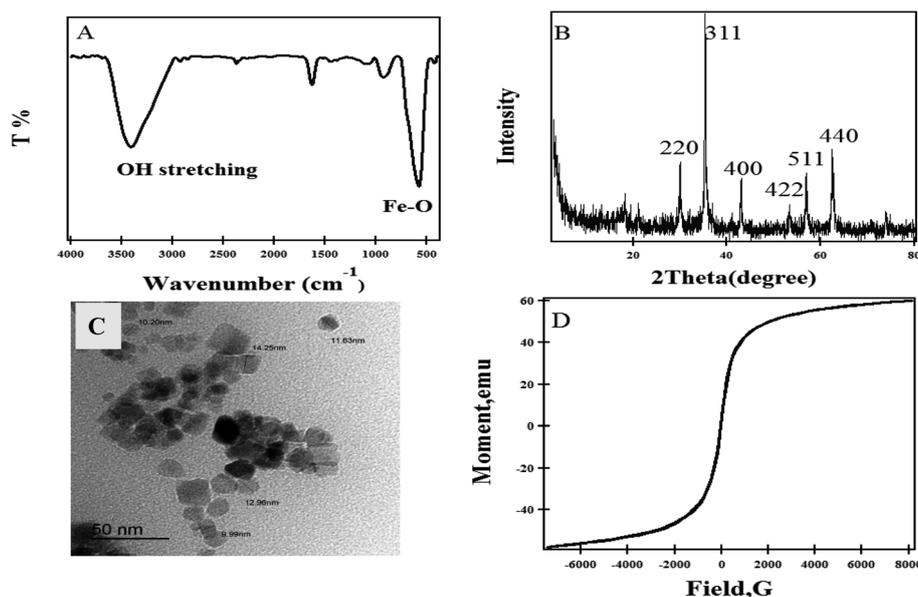

Fig. 2 (A) FTIR spectrum, (B) XRD pattern, (C) TEM of MNP and (D) magnetization *versus* the applied magnetic field at room temperature of MNPs.
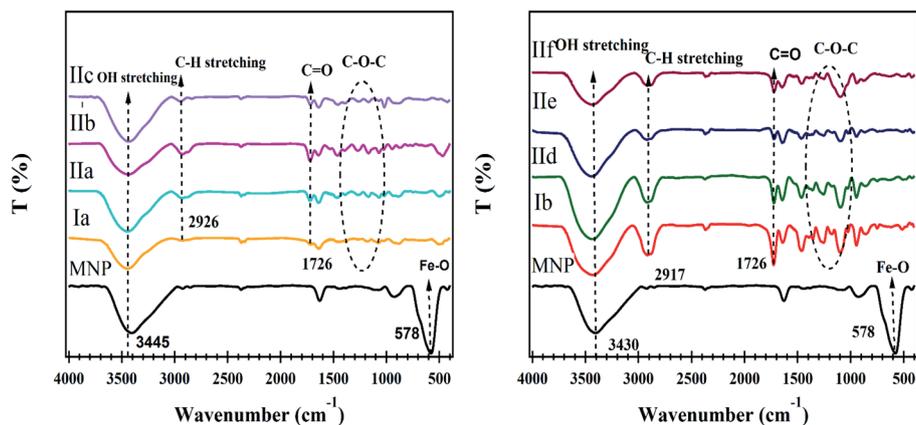
Fig. 3 FT-IR spectra of hydrogel I_a, I_b and their nanocomposites $II_{(a-f)}$.

The FT-IR spectra of hydrogel polymers $I_{a,b}$ (Fig. 3) display a very strong peak at 1726 cm^{-1} arising from the C=O stretching of the ester group. Bands are observed in the range from 1177–1075 cm^{-1} corresponding to the C–O–C stretching vibrations. The peaks at 2926 and 2917 cm^{-1} are associated with the stretching C–H bands, and broad absorption bands at higher wavenumbers of 3444 and 3430 cm^{-1} are due to the OH linked to hydrophilic polymeric chains in I_a, I_b, respectively. The spectra of the II_{a-f} hydrogel nanocomposites show that the peaks assigned to the OH stretching at 3444 and 3430 cm^{-1} were shifted to 3445, 3436, 3433, 3436, 3442, and 3439 cm^{-1} in II_{a-f}, respectively, and the characteristic peak of the carbonyl of the ester group at 1726 was shifted to 1725, 1721, 1719,1724, 1725, and 1725 cm^{-1} in II_{a-f}, respectively. The shift may arise from the interaction between the hydrogel and MNPs.

The XRD pattern of I_a includes two broad peaks at 12.65° and 19.1° and for I_b, a broad beak at 18.15° is observed which indicates that the polymers are in the amorphous form (Fig. 4).
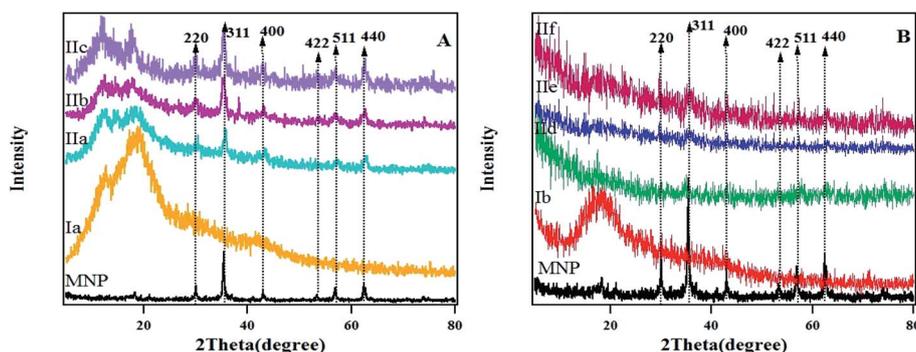

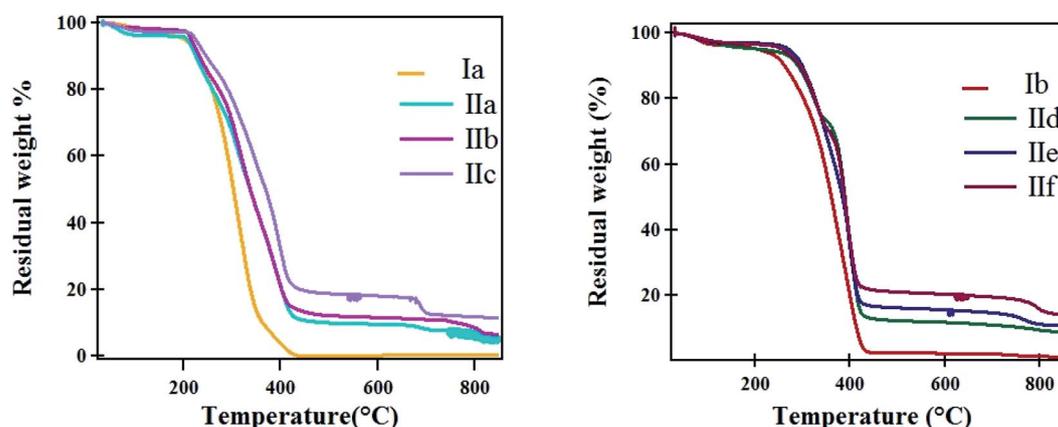**Fig. 4** XRD patterns of MNPs, hydrogel $I_{a,b}$ and their nanocomposites II_{a-f}.

Fig. 5 TGA thermograms of hydrogels $I_{a,b}$ and their hydrogel nanocomposites II_{a-f}.

The spectra show peaks at $2\theta = 29.97°$, $35.37°$, $43°$, $53.31°$, $56.88°$ and $62.46°$ for the magnetic hydrogel nanocomposite ($\mathbf{II_{a-c}}$), which are assigned to the (220), (311), (400), (422), (511) and (440) crystalline phase for Fe_3O_4. The average crystallite size was roughly calculated for (MNPs) according to Scherrer equation[37] to be 23.9 nm.

The thermograms (Fig. 5) of the prepared hydrogels and magnetic hydrogel nanocomposites reveal two stages of decomposition. The first stage occurred at a temperature range from 30 °C up to 200 °C. In this stage, the loss of absorbed water ranged from 2 to 6%. The second stage is due to the thermal decomposition of the polymers starting from 225 °C up to 450 °C with weight loss ranging from 65% to 84%.

The thermal analyses of the prepared samples are illustrated in Table 2. The temperature at different weight loss percentages (T-2, T-5, T-10, T-40, T-50, and T-60%) and the residual at 800 °C were calculated. The data in the table showed that the weight losses due to decomposition temperature ranged from 70 to 84% in the temperature range from ~220 °C to ~470 °C. It was found that the residuals at 800 °C are nearly identical with the weight ratio used in the preparation conditions.

It was found from the degradation temperature that samples $\mathbf{I_b}$ and $\mathbf{II_{d-f}}$ are more thermally stable than samples $\mathbf{I_a}$ and $\mathbf{II_{a-c}}$. This was attributed to the presence of a longer oligo(oxyethylene) group, which led to a more stable residual and later degradation process. In addition, the degradation temperature was increased with increasing amounts of Fe_3O_4 nanoparticles in the polymer samples, and this means that greater thermal stability is achieved. Furthermore, by increasing the Fe_3O_4 nanoparticles content in the polymer matrix, the formation of carbon residues is increased and this can explain the high heat capacity of the $\mathbf{II_{d-f}}$ nanocomposites.

Magnetic hydrogels can be used in hyperthermia, which is one of the effective methods for cancer treatment.[38] When the MNPs are exposed to an external magnetic field, they absorb energy and cause a local temperature increase above 43 °C. This leads to the destruction of cancer cells, while healthy cells will survive.[5,39] The measured magnetization curves at room temperature for MNPs, $\mathbf{II_c}$ and $\mathbf{II_f}$ are shown in Fig. 6. It can be seen that the saturation magnetization for MNPs, IIc and $\mathbf{II_f}$ are 60.06, 48.28 and 10.45 emu g^{-1}, respectively. There was no hysteresis in the magnetization of the samples, indicating that the produced magnetic particles are superparamagnetic. The

magnetic hydrogels saturation magnetization values were smaller than the values of the pure magnetic nanoparticles. This is caused by the presence of a diamagnetic polymer around the magnetic nanoparticles that quenches the magnetic moment. Super magnetic behaviors have been exposed by both of them, indicating the incorporation of magnetic nanoparticles into the composite particles, with no residual effect of hysteresis loops in the applied magnetic field.

The surface morphologies of the prepared hydrogel ($\mathbf{I_a}$) and magnetic hydrogel nanocomposite ($\mathbf{II_c}$) were distinguished by using SEM. The morphology of the hydrogels was noticed at different scales, as shown in Fig. 7(A and B). The morphology of the hydrogels shows that there are dense, rough, tight, and wavy surfaces. This refers to its dense cross-linking. The cross-sectional images of the magnetic hydrogel ($\mathbf{II_c}$) nanocomposites, shown in Fig. 7(C and D), confirm a wrinkled, rough morphology with tiny nanoparticles, which may arise from the incorporation of iron oxide nanoparticles. This comparatively rough surface is convenient for the diffusion of the drug, which enhances the drug loading efficacy.

TEM images of the magnetic hydrogels ($\mathbf{II_b}$, $\mathbf{II_c}$, $\mathbf{II_e}$, $\mathbf{II_f}$) are shown in Fig. 8A–D, respectively. In the TEM image, the black spheres and cubes are attributed to Fe_3O_4 nanoparticles. It is clearly visible from Fig. 8 that iron oxide nanoparticles were well dispersed through the polymer matrix in some regions, and tend to aggregate in other regions.
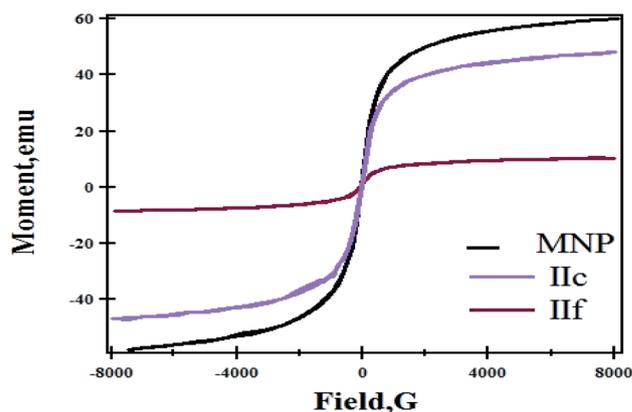

Fig. 6 Magnetization curves of MNP, II_c, and II_f.

Table 2 TGA data of the samples $I_{a,b}$ and II_{a-f}

| Sample	T-2%	T-5%	T-10%	T- 40%	T-50%	T-60%	Residual (%) at 800 °C
$\mathbf{I_a}$	107.77	200.87	229.29	290.88	302.6	313.88	0.57
$\mathbf{II_a}$	63.99	207.21	224.7	315.13	336.92	359.08	6.03
$\mathbf{II_b}$	151.71	215.61	232.17	318.57	337.26	359.66	8.65
$\mathbf{II_c}$	84.81	224.2	246.1	344.72	368.75	387.89	11.89
$\mathbf{I_b}$	78.41	206.87	261.95	346.25	360.41	373.75	1.44
$\mathbf{II_d}$	88.58	215.21	290.02	380.7	389.06	396.49	9.44
$\mathbf{II_e}$	90.02	271.33	298.72	367.25	383.99	395.46	11.27
$\mathbf{II_f}$	94.82	258.22	294.78	378.72	388.23	396.92	15.83
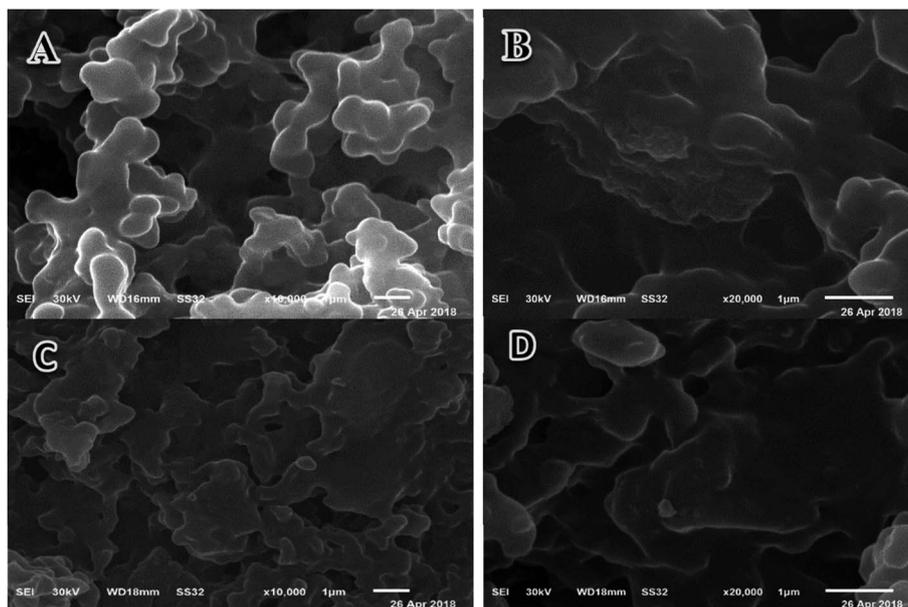
Fig. 7 SEM images of hydrogel I_a (A, B) and magnetic hydrogel nanocomposite II_c (C, D).
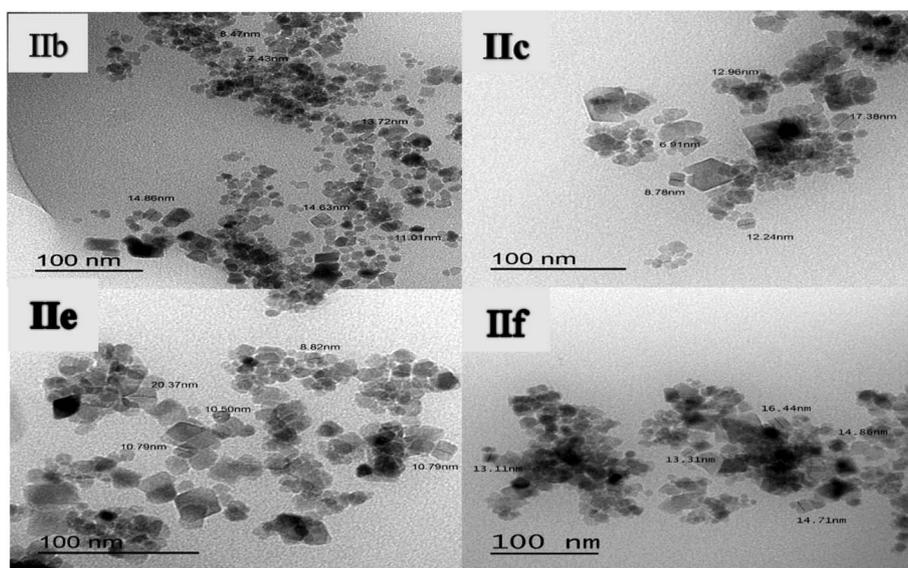

Fig. 8 TEM images of the hydrogel nanocomposites.

3.1. Drug loading onto carriers

To investigate the optimum condition of drug loading onto the hydrogels ($I_{a,b}$), different conditions were studied, such as the drug concentration, temperature, and pH medium (Table 3). It was observed that there is no loading in acidic or basic medium at the tested temperatures, and the most efficient concentration of drug was found at 16 ppm (loading 53.4% onto the I_a polymer) and loading reduced with increasing temperature. However, for I_b, the most suitable conditions for maximum loading was observed at 16 ppm, 43 °C. The optimum conditions were used for loading the magnetic hydrogels

nanocomposites (II_{a-f}), and the loading percentage (54–58%) was enhanced with increasing Fe_3O_4 contents.

3.2. Release studies of norfloxacin

The release rate of the NOR drug from the prepared carriers-loaded NOR was studied with respect to the effect of the polymer structure, the percentage of loaded drug, the ratios of the MNPs, temperature and the pH of the aqueous medium.

Fig. 9 shows the release profile of NOR from IV_h, IV_i, IV_j, and IV_k. An initial burst release was observed from all of the hydrogel-loaded drugs. The rate of NOR release from IV_h, IV_i, IV_j, IV_k continued to reach 100% after 194, 178, 352, 240 h at pH

Table 3 Loading of NOR on MNPs, hydrogels and magnetic hydrogel nanocomposites

Loaded carrier code	Carrier code	NOR Conc. (ppm)	Temperature (°C)	Medium	Loading (%)
III_a	MNP	16	28	Dist. H_2O	88.28
IV_a	I_a	16	28	Dist. H_2O	53.4
IV_b	I_a	16	43	Dist. H_2O	31.45
IV_c	I_a	16	55	Dist. H_2O	27.5
IV_d	I_a	16	65	Dist. H_2O	10.22
IV_e	I_a	16	28	pH = 2	0
IV_f	I_a	16	28	pH = 10	0
IV_g	I_b	16	28	Dist. H_2O	14
IV_h	I_b	8	43	Dist. H_2O	45.12
IV_i	I_b	10	43	Dist. H_2O	41.46
IV_j	I_b	16	43	Dist. H_2O	63
IV_k	I_b	20	43	Dist. H_2O	44.87
IV_l	I_b	16	55	Dist. H_2O	13.28
IV_m	I_b	16	65	Dist. H_2O	12.31
IV_n	I_b	16	28	pH = 2	0
IV_o	I_b	16	28	pH = 10	0
V_a	II_a	16	28	Dist. H_2O	57.893
V_b	II_b	16	28	Dist. H_2O	58.310
V_c	II_c	16	28	Dist. H_2O	63.485
V_d	II_d	16	43	Dist. H_2O	54.346
V_e	II_e	16	43	Dist. H_2O	55.100
V_f	II_f	16	43	Dist. H_2O	55.987

7.4, respectively. It is worth mentioning that the highest loaded carrier, IV_j, shows sustained release over a period of 352 h.

Fig. 10 displays the release profile of NOR from different carriers at different pHs buffer solutions. In general, the sample III_a was distinguished by faster initial release in the first few days, followed by a moderate, gradual release. The rate of NOR release from III_a was persistent to reach 67% after 243 h at pH 5.4, 148 h at pH 6.7 and 76 h at pH 7.4, respectively. However, a sustained release was observed for the hydrogel and magnetic hydrogel nanocomposites. The rate of NOR release from IV_a and IV_j continued to reach 100% after 888, 440 h at pH 5.4; 720, 390 h at pH 6.7; and 648, 352 h at pH 7.4, respectively. The rate of NOR release from V_c and V_f continued to reach 100% after 1111, 845 h at pH 5.4; 976, 773 h at pH 6.7; and 871, 702 h at pH 7.4, respectively. The rate of release of NOR from different

Fig. 9 *In vitro* release of NOR from IV_h, IV_i, IV_j, and IV_k in normal buffer solution at pH = 7.4.

magnetite contents carriers shows that the release from V_a, V_b, and V_c continued to reach 100% after 941, 1003, 111 h at pH 5.4; and 792, 888, 967 h at pH 6.7; and 696, 768, 871 h at pH 7.4. In addition, the same trend was observed with increasing content of magnetite, the rate of release from V_d, V_e, and V_f continued to reach 100% after 685, 766, 845 h at pH 5.4; 576, 690, 773 at pH 6.7; and 502, 600, 702 h at pH 7.4, respectively. It is worth mentioning that magnetic nanoparticles not only produce magnetothermal for direct killing effect, but also act as a trigger to enhance the drug release.[40,41] "In our study, the inclusion of magnetite nanoparticles into the hydrogel slows down the release, and increasing the percentage in the nanocomposites extends the time of release."

All systems showed significantly faster release in basic media (pH = 7.4). The order of release found was as follows: pH = 7.4 > pH = 6.7 > pH = 5.4. This may be due to the increasing solubility of NOR by increasing the pH of the medium. In addition, it was established that the drug release from the prepared samples occurs during the time period of 15–40 days. It was reported that the lipid-polylactic hybrid nanoparticles loaded norfloxacin showed initially burst release followed by sustained drug release with a maximum of 67.4–89.7% in 24 h, depending on the formulation.[42] A magnetic thermosensitive hydrogel was developed as an intravesical *Bacillus* Calmette–Guérin (BCG) delivery system,[43] and characterized by high antitumor efficacy with a continuous release of BCG up to 48 h. The additions of NaCl to the solution (pH 6.7) affect the release rate of the NOR from IV_a [Fig. 10G], and it becomes slower because of the increase in ionic strength. Interestingly, the release from V_b (58.3% loading) at pH values of 6.7 and 5.4 is slower than that of V_e (55.1% loading). By increasing the temperature of the
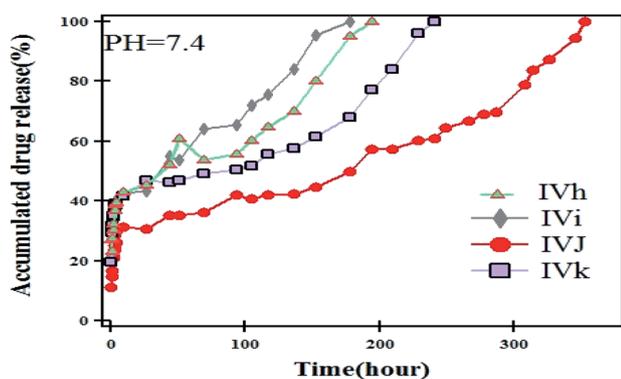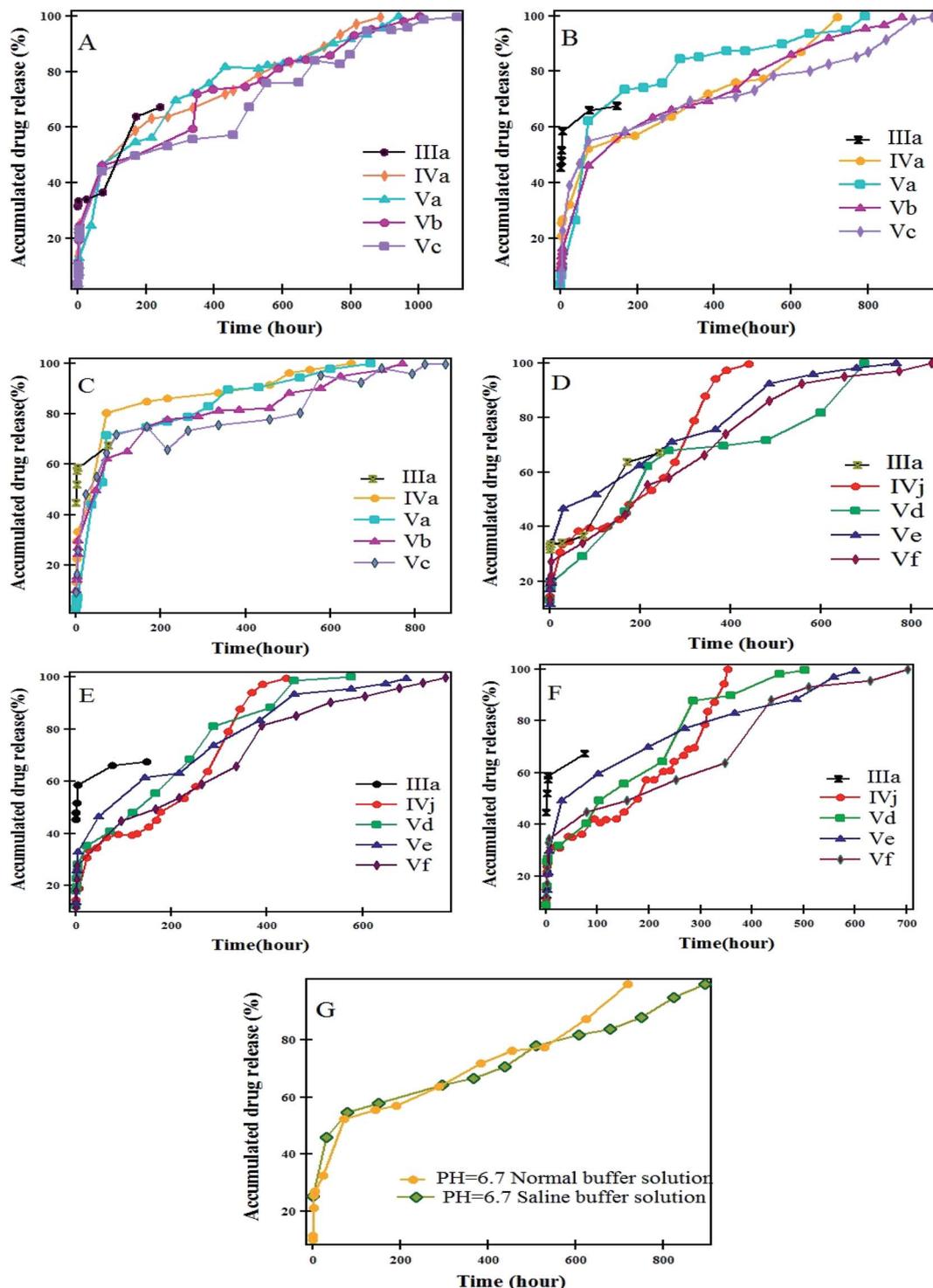
Fig. 10 *In vitro* release of NOR from III_a, IV_a, and $V_{(a-c)}$ nanocomposites in a normal buffer solution at pH = 5.4 (A), pH = 6.7 (B), and pH 7.4 (C). *In vitro* release of NOR from III_a, IV_j and $V_{(d-f)}$ nanocomposites in a normal buffer solution at pH = 5.4 (D), pH = 6.7 (E), and pH 7.4 (F), in normal and saline buffer solution for sample IV_a at pH = 6.7 (G).

medium to 50 °C, the burst release happened and almost 50–75% of the drug was released within 24 h, as shown in Fig. 11.

The release kinetics of V_c was studied in order to identify the release mechanism. The release data were tested by applying the following model equations:

Zero-order release kinetics:[44]

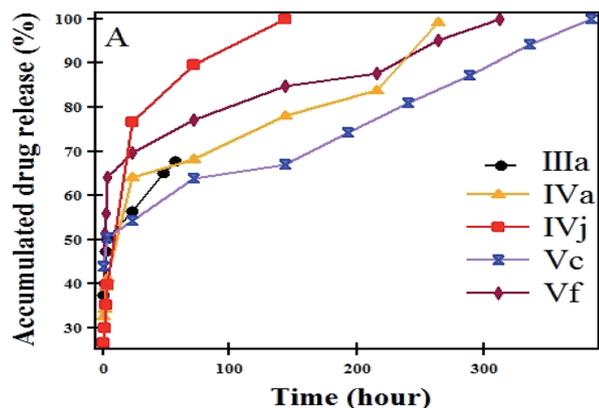$$W = W_0 + k_1 t \qquad (2)$$

First-order release kinetics:[45]

Fig. 11 *In vitro* release of NOR at 50 °C from III_a, IV_a, IV_j, V_c and V_f nanocomposites in a normal buffer solution at pH = 5.4.

$$\log(100 - W) = \log 100 - k_2 t \tag{3}$$

Higuchi-kinetics:[46]

$$W = k_3 t^{1/2} \tag{4}$$

Hixson–Crowell Kinetics:[47]

$$(100 - W)^{1/3} = 100^{1/3} - k_4 t \tag{5}$$

Korsemeyer–Peppas equation:[48]

$$M_t/M_\infty = k_5 t^n \tag{6}$$

where K_1, K_2, K_3, and K_4 are the drug release rate constants for zero-order, first-order, Higuchi and Hixson–Crowell models, W is the proportion of released NOR at time t, and K_5 is a constant that integrates the structural and geometric properties of the drug.

The kinetic mechanism of the release process was investigated by applying kinetic model equations eqn (2)–(6). The parameters of the release kinetics, such as regression coefficient (R^2), rate constant (K), release exponent value (n) and the slope for each model, are graphically determined for all models, and are collected in Table 4. The data in the table suggest that the release of the drug was found to follow Hixson–Crowell kinetics, rather than other models in pH = 5.4, and follow Higuchi kinetics rather than other models at pH = 6.7 and 7.4. From the Korsmeyer–Peppas equation at pHs (5.4, 6.7 and 7.4) media, the release mechanism follows the Fickian diffusion mechanism.

The antibacterial activities of the free carriers and loaded NOR were tested against four human pathogens: *Staphylococcus aureus*, *Streptococcus* (Gram-positive bacteria) and *E. coli*, and *Klebsiella pneumonia* (Gram-negative bacteria). The inhibition zone (ZOI) resulting from each sample was measured after 24 h incubation at 37 °C (Table 5). MNPS showed antibacterial

Table 4 Kinetic parameters for the magnetic hydrogel nanocomposite V_c

Release medium	Zero order		1st order		Higuchi		Hixson–Crowell		Korsmeyer–Peppas		
	K_1	R^2	K_2	R^2	K_3	R^2	K_4	R^2	K_5	R^2	n
pH 7.4	0.0749	0.727	−0.002	0.830	0.031	0.945	−0.003	0.896	0.837	0.930	0.295
pH 6.7	0.0785	0.907	−0.001	0.7387	0.030	0.950	−0.003	0.892	−1.157	0.929	0.395
pH 5.4	0.0825	0.920	−0.002	0.834	0.030	0.946	−0.003	0.955	−1.210	0.945	0.398

Table 5 Inhibition zones (mm) of NOR, free and loaded carrier against different microorganisms

Sample	*E. coli*	*Streptococcus*	*Klebsiella pneumonia*	*Staphylococcus*
NOR	16 ± 0 mm	40 ± 0 mm	25 ± 0 mm	39 ± 0 mm
MNP	11.5 ± 0 mm	35.5 ± 0 mm	14.5 ± 0 mm	−ve
I_a	−ve	18 ± 0.5 mm	−ve	−ve
II_a	−ve	17 ± 0 mm	−ve	−ve
II_b	−ve	10 ± 0.5 mm	−ve	−ve
II_c	−ve	23 ± 2 mm	−ve	−ve
I_b	15 ± 1 mm	12.5 ± 0.5 mm	17 ± 0 mm	9 ± 0.3 mm
II_d	−ve	−ve	−ve	−ve
II_e	−ve	−ve	−ve	−ve
II_f	−ve	−ve	−ve	−ve
IV_a	15 ± 1 mm	29 ± 0.8 mm	15 ± 0 mm	−ve
V_a	16 ± 0.25 mm	34 ± 4 mm	26.1 ± 1 mm	10 ± 0 mm
V_b	24.45 ± 2.15 mm	24 ± 0.3 mm	25 ± 1.32 mm	−ve
V_c	−ve	35 ± 3 mm	24.05 ± 1 mm	−ve
IV_j	23 ± 1 mm	19 ± 0.6 mm	18 ± 0.25 mm	14 ± 1.02 mm
V_d	−ve	−ve	13.1 ± 0.5 mm	−ve
V_e	16 ± 1.3 mm	27 ± 2.5 mm	15 ± 3 mm	−ve
V_f	14 ± 0.8 mm	13.25 ± 1.5 mm	21.3 ± 1 mm	−ve

Paper

efficacy against *E. coli*, *Klebsiella pneumonia* and *Streptococcus*. Interestingly **I$_b$** showed unique powerful activity against *Klebsiella pneumonia*, *E. coli* and *Staphylococcus aureus* however, **I$_a$** showed no activity against them. The antibacterial efficacy of the loaded hydrogels (**IV$_a$**, **IV$_j$**) and magnetic hydrogel (**V$_{a-f}$**) nanocomposites showed excellent activity compared to the unloaded drug, which indicated the efficacy of the prepared nanocomposites.

The result of the anti-microbial efficacy of the lipid polylactic acid nanohybrid loaded with NOR showed good antibacterial efficacy towards *Pseudomonas aeruginosa* (Gram-negative bacteria) with ZOI ranging from 11 to 21 mm, and moderate efficacy towards *Staphylococcus aureus* (Gram-positive bacteria) with ZOI 7–15 mm, depending on the concentration of the nanocarrier (2–8 µg mL^{-1}).[42]

Some antibacterial quinolones have been reported to employ their efficacy by targeting both Gram-positive bacteria topo-isomerase IV and Gram-negative bacteria DNA gyrase,[49] and inhibiting the process of DNA replication.[50] NOR exerts its influence by inhibition of two kinds of enzymes, topoisomerase IV and DNA gyrase.[51] DNA topoisomerases are found in both prokaryotic and eukaryotic cells, and are a target for chemo-therapeutic medication in anticancer and antibacterial therapies.[52] These enzymes perform critical tasks in many basic nuclear processes,[53] and are necessary for eukaryotic cells survival.[54]

In fact, the enzyme DNA topoisomerase II stimulates the breakage of the DNA double strand to allow strand passage, and thus controls the conformation and topology of DNA.[55]

The cytotoxic activity of NOR, MNP and carriers-loaded NOR (**III$_a$**, **IV$_a$**, **IV$_j$** and **V$_{(a-f)}$**) was investigated *in vitro* compared to DOX against four cancer cell lines (HCT-116, MCF-7, HepG-2 and PC3) using the MTT colorimetric assay. The inhibitory activities of compounds NOR, MNP, **III$_a$**, **IV$_a$**, **IV$_j$** and **V$_{(a-f)}$** nanocomposites *versus* the cell lines are shown in Table 6 as IC50 values, along with relevant mean values. The IC50 values of **III$_a$** towards all cancer cell lines indicate that **III$_a$** possessed poor activity with the exclusion of the PC3 tumor cell line that showed the non-cytotoxicity against this cell line (IC50 > 100 µM). In addition, the IC50 values towards all cancer cell lines indicate that **IV$_a$** possessed very strong activity with regard to Doxorubicin. In addition, the IC50 values of **IV$_j$** and **V$_b$** towards all cancer cell lines indicate that all these compounds possessed strong activity with respect to Doxorubicin. It is worthy to note that **IV$_a$** and **V$_b$** showed a higher activity than free NOR and MNP with respect to Doxorubicin. In contrast, **IV$_j$**, **V$_a$**, **V$_c$**, **V$_d$**, **V$_e$** and **V$_f$** nano-composites showed moderate activity towards all tested cell lines.

In addition, the MNPs and **II$_c$** nanocomposite were examined against the normal human cell line (WISH). The obtained results showed that the MNPs and **II$_c$** had IC50 (94.12 ± 5.4, 69.61 ± 3.5 µg mL^{-1}) more than the control drug DOX (6.72 ± 0.5 µg mL^{-1}), indicating the selectivity of action towards cancer cells, as well as a shortage of cytotoxicity towards healthy cells.

Table 6 Cytotoxic activity of some compounds towards human cancer cells

		In vitro cytotoxicity IC50 (µg mL^{-1})[a]			
No.	Comp.	HePG2	HCT-116	MCF-7	PC3
	DOX	4.50 ± 0.2	5.23 ± 0.3	4.17 ± 0.2	8.87 ± 0.6
A	NOR	14.30 ± 1.2	23.62 ± 1.8	20.47 ± 1.6	34.94 ± 2.5
B	**MNP**	**38.53 ± 2.5**	**52.02 ± 3.1**	**45.25 ± 2.8**	**71.86 ± 3.4**
C	**III$_a$**	88.34 ± 4.2	92.13 ± 4.9	71.39 ± 3.5	>100
D	**IV$_a$**	7.83 ± 0.6	10.48 ± 0.9	9.37 ± 0.7	15.29 ± 1.3
E	**V$_a$**	32.22 ± 2.3	48.27 ± 2.8	25.16 ± 1.9	43.38 ± 2.9
F	**V$_b$**	11.61 ± 1.0	13.56 ± 1.2	14.85 ± 1.1	20.70 ± 1.6
G	**V$_c$**	23.09 ± 1.9	30.54 ± 2.3	21.20 ± 1.7	39.04 ± 2.5
H	**IV$_j$**	18.57 ± 1.4	16.71 ± 1.4	19.64 ± 1.5	28.72 ± 2.1
I	**V$_d$**	26.24 ± 1.5	33.75 ± 1.9	25.45 ± 2.0	39.26 ± 2.4
J	**V$_e$**	36.18 ± 2.5	48.19 ± 1.2	29.30 ± 1.8	52.75 ± 2.6
K	**V$_f$**	49.68 ± 2.8	54.89 ± 3.1	34.18 ± 2.4	75.19 ± 3.5

[a] IC50 (µg mL^{-1}): 1–10 (very strong). 11–20 (strong). 21–50 (moderate). 51–100 (weak) and above 100 (non-cytotoxic).

4 Conclusion

Antitumor nanocarriers with antimicrobial analogs were prepared *via* radical polymerization of oligo(oxyethylene) methacrylate in the presence of Fe$_3$O$_4$ nanoparticles. A magnetic spherical and cuboid shaped of MNPs with an average particle size of 15 nm were dispersed in the hydrogels. A sustained NOR drug release was observed at different pH values. However, by increasing temperature, a burst release was observed. It was found that the drug release followed the Hixson–Crowell kinetics at pH = 5.4, and Higuchi kinetics at pH = 6.7 and 7.4. From the Korsmeyer–Peppas equation in pH media (5.4, 6.7 and 7.4), the release mechanism follows the Fickian diffusion mechanism. Furthermore, these nanodrugs had high anticancer efficacy against cancer cell lines, and were free of cytotoxicity against healthy cells. The permutation of an effective activity against bacteria and cancer cell lines, coupled with a dearth of cytotoxicity against healthy cells, make these factors important in the search for new potential antimicrobials capable of minimizing bacterial infection risks in cancer patients who are frequently immunocompromised. More studies are underway to evaluate the promising double-acting chemotherapeutics of the nanodrugs *in vivo*.

Conflicts of interest

There are no conflicts to declare.

References

1 A. S. Hoffman, *Ann. N. Y. Acad. Sci.*, 2001, **944**, 62–73.
2 T. R. Hoare and D. S. Kohane, *Polymer*, 2008, **49**, 1993–2007.
3 C. Sutton, *Obstet. Gynecol.*, 2005, **7**, 168–176.
4 S. Davaran, S. Alimirzalu, K. Nejati-Koshki, H. T. Nasrabadi, A. Akbarzadeh, A. A. Khandaghi, M. Abbasian and S. Alimohammadi, *Asian Pac. J. Cancer Prev.*, 2014, **15**, 49–54.

5 J. Zhang, Q. Huang and J. Du, *Polym. Int.*, 2016, **65**, 1365–1372.

6 Z. Liu, H. Wang, B. Li, C. Liu, Y. Jiang, G. Yu and X. Mu, *J. Mater. Chem.*, 2012, **22**, 15085–15091.

7 M. Babincová, D. Leszczynska, P. Sourivong, P. Čičmanec and P. Babinec, *J. Magn. Magn. Mater.*, 2001, **225**, 109–112.

8 J. I. Kim, C. Chun, B. Kim, J. M. Hong, J.-K. Cho, S. H. Lee and S.-C. Song, *Biomaterials*, 2012, **33**, 218–224.

9 E. Yarar, G. Karakas, D. Rende, R. Ozisik and S. Malta, *APS March Meeting Abstracts*, 2016, p M1. 090.

10 L. Zhang, W.-F. Dong and H.-B. Sun, *Nanoscale*, 2013, **5**, 7664–7684.

11 H. Zhao, K. Saatchi and U. O. Häfeli, *J. Magn. Magn. Mater.*, 2009, **321**, 1356–1363.

12 Y. P. Yew, K. Shameli, M. Miyake, N. B. B. A. Khairudin, S. E. B. Mohamad, T. Naiki and K. X. Lee, *Arab. J. Chem.*, 2020, **13**(1), 2287–2308.

13 M. Ahmed and M. Douek, *Biomed Res. Int.*, 2013, **2013**, 281230.

14 A. Singh, F. Dilnawaz, S. Mewar, U. Sharma, N. Jagannathan and S. K. Sahoo, *ACS Appl. Mater. Interfaces*, 2014, **6**, 4595.

15 H. Maeda, *Adv. Enzym. Regul.*, 2001, **41**, 189–207.

16 M. Wu and S. Huang, *Mol. Clin. Oncol.*, 2017, **7**, 738–746.

17 G. Giani, S. Fedi and R. Barbucci, *Polym*, 2012, **4**, 1157–1169.

18 B. Gaihre, M. S. Khil, D. R. Lee and H. Y. Kim, *J. Pharmacol.*, 2009, **365**, 180–189.

19 J. Chomoucka, J. Drbohlavova, D. Huska, V. Adam, R. Kizek and J. Hubalek, *Pharmacol. Res.*, 2010, **62**, 144–149.

20 Y. Y. Liang, L. M. Zhang, W. Jiang and W. Li, *ChemPhysChem*, 2007, **8**, 2367–2372.

21 H. Liu, C. Wang, Q. Gao, J. Chen, B. Ren, X. Liu and Z. Tong, *Int. J. Pharm.*, 2009, **376**, 92–98.

22 W. Zhao, K. Odelius, U. Edlund, C. Zhao and A.-C. Albertsson, *Biomacromolecules*, 2015, **16**, 2522–2528.

23 Y. Zhou, N. Sharma, P. Deshmukh, R. K. Lakhman, M. Jain and R. M. Kasi, *J. Am. Chem. Soc.*, 2012, **134**, 1630–1641.

24 P. Ilg, *Soft Matter*, 2013, **9**, 3465–3468.

25 S. van Berkum, P. D. Biewenga, S. P. Verkleij, J. B. van Zon, K. W. Boere, A. Pal, A. P. Philipse and B. H. Erné, *Langmuir*, 2015, **31**, 442–450.

26 N. Satarkar and J. Hilt, *Acta Biomater.*, 2008, **4**, 11–16.

27 R. A. Frimpong, S. Fraser and J. Zach Hilt, *J. Biomed. Mater. Res. A: An Official Journal of The Society for Biomaterials*, The Japanese Society for Biomaterials, and The Australian Society for Biomaterials and the Korean Society for Biomaterials, 2007, vol. 80, pp. 1–6.

28 W.-T. Liu, *J. Biosci. Bioeng.*, 2006, **102**, 1–7.

29 P. M. Xulu, G. Filipcsei and M. Zrínyi, *Macromolecules*, 2000, **33**, 1716–1719.

30 M. Zrınyi, D. Szabó and H.-G. Kilian, *Polym. Gels Netw.*, 1998, **6**, 441–454.

31 R. Hergt, S. Dutz, R. Müller and M. Zeisberger, *J. Phys. Condens. Matter*, 2006, **18**, S2919.

32 J.-K. Yang, J.-H. Yu, J. Kim and Y.-H. Choa, *Mater. Sci. Eng. A*, 2007, **449**, 477–479.

33 J. Li and K. Kataoka, *J. Am. Chem. Soc.*, 2021, **143**, 538–559.

34 P. Loekitowati Hariani, M. Faizal, R. Ridwan, M. Marsi and D. Setiabudidaya, *Int. J. Environ. Sci. Develop.*, 2013, **4**, 336–340.

35 J. H. Jorgensen and J. D. Turnidge, in *Manual of Clinical Microbiology*, American Society of Microbiology, 11th edn, 2015, pp. 1253–1273.

36 T. Mosmann, *J. Immunol. Methods*, 1983, **65**, 55–63.

37 C. Hammond, *The Basics of Crystallography and Diffraction*, Oxford University Press, 2nd edn, 2001, ISBN-13: 978-0198505525, ISBN-10: 0198505523.

38 A. L. Daniel-da-Silva, R. S. Carvalho and T. Trindade, *Recent Pat. Nanotechnol.*, 2013, **7**, 153–166.

39 A. K. Gupta and M. Gupta, *Biomaterials*, 2005, **26**, 3995–4021.

40 J. Li, Y. Anraku and K. Kataoka, *Angew. Chem., Int. Ed.*, 2020, **59**, 13526–13530.

41 J. Li, Y. Li, Y. Wang, W. Ke, W. Chen, W. Wang and Z. Ge, *Nano Lett.*, 2017, **17**, 6983–6990.

42 V. Dave, R. B. Yadav, K. Kushwaha, S. Yadav, S. Sharma and U. Agrawal, *Bioact. Mater.*, 2017, **2**, 269–280.

43 D. Zhang, P. Sun, P. Li, A. Xue, X. Zhang, H. Zhang and X. Jin, *Biomaterials*, 2013, **34**, 10258–10266.

44 M. A. Kalam, M. Humayun, N. Parvez, S. Yadav, A. Garg, S. Amin, Y. Sultana and A. Ali, *Cont. J. Pharm. Sci.*, 2007, **1**, 30–35.

45 J. G. Wagner, *J. Pharm. Sci.*, 1969, **58**, 1253–1257.

46 T. Higuchi, *J. Pharm. Sci.*, 1963, **52**, 1145–1149.

47 A. Hixson and J. Crowell, *Ind. Eng. Chem.*, 1931, **23**, 923–931.

48 R. W. Korsmeyer, R. Gurny, E. Doelker, P. Buri and N. A. Peppas, *Int. J. Pharm.*, 1983, **15**, 25–35.

49 D. C. Hooper, *Clin. Infect. Dis.*, 1998, **27**, S54–S63.

50 L. M. Wentzell and A. Maxwell, *J. Mol. Biol.*, 2000, **304**, 779–791.

51 A. V. Shindikar and C. Viswanathan, *Bioorg. Med. Chem. Lett*, 2005, **15**, 1803–1806.

52 V. T. Andriole, *Clin. Infect. Dis.*, 2005, **41**, S113–S119.

53 A. K. McClendon and N. Osheroff, *Mutat. Res. Fund. Mol. M.*, 2007, **623**, 83–97.

54 S. Elsea, N. Osheroff and J. Nitiss, *J. Biol. Chem.*, 1992, **267**, 13150–13153.

55 E. Willmore, S. de Caux, N. J. Sunter, M. J. Tilby, G. H. Jackson, C. A. Austin and B. W. Durkacz, *Blood*, 2004, **103**, 4659–4665.